

PAPER • OPEN ACCESS

## An experimental apparatus to measure soot morphology at high pressures using multi-angle light scattering

To cite this article: Hafiz M F Amin and William L Roberts 2019 *Meas. Sci. Technol.* **30** 075902

View the [article online](#) for updates and enhancements.

### You may also like

- [Agent-based evacuation model incorporating life jacket retrieval and counterflow avoidance behavior for passenger ships](#)  
Baocheng Ni, Zhuang Lin and Ping Li
- [A layer-peeling method for signal trapping correction in planar LII measurements of statistically steady flames](#)  
F Escudero, J J Cruz, F Liu et al.
- [Study of Water Balance in a Polymer Electrolyte Fuel Cell by Locally Resolved Impedance Spectroscopy](#)  
I. A. Schneider, H. Kuhn, A. Wokaun et al.

# An experimental apparatus to measure soot morphology at high pressures using multi-angle light scattering

Hafiz M F Amin<sup>1</sup>  and William L Roberts

Clean Combustion Research Center, King Abdullah University of Science and Technology (KAUST), Thuwal, 23955-6900, Saudi Arabia

E-mail: [hafiz.amin@kaust.edu.sa](mailto:hafiz.amin@kaust.edu.sa)

Received 15 January 2019, revised 29 March 2019

Accepted for publication 24 April 2019


Published 14 June 2019



## Abstract

In this work, a novel experimental setup is described which is designed and built specifically to study soot morphology using light scattering and extinction techniques at elevated pressures. The experimental setup consists of a counterflow burner housed inside a pressure vessel. A unique feature of this pressure vessel is the four curved optical windows which can provide the required optical access for light scattering measurements in order to infer the morphological parameters of soot. Using this setup,  $N_2$ -diluted ethylene and air counterflow flames are stabilized from 3 to 5 atm. Global strain rate ( $a$ ) of  $30\text{ s}^{-1}$  is maintained at all conditions and all the flames studied are soot formation (SF) flames. Light scattering by soot is measured between  $15^\circ$  to  $165^\circ$  at different locations along the axis of the burner. Ratio of total scattering to absorption ( $\rho_{sa}$ ), path averaged soot volume fraction ( $f_v$ ), mean primary particle size ( $d_p$ ), mean radius of gyration of aggregates ( $R_{gm}$ ) and fractal dimension ( $D_f$ ) are calculated from multi-angle light scattering and extinction data using Rayleigh–Debye–Gans theory for fractal aggregates (RDG-FA).  $\rho_{sa}$ ,  $f_v$ ,  $d_p$ , and  $R_{gm}$  increase as the pressure is raised. The scattering contribution in these measurements vary from 1.3% to 16% of absorption which suggests that wide angle optical access is essential for accurate measurements of  $f_v$ .  $D_f$  equal to 1.27 is measured near the flame at 3 atm which increases as the particles are convected away from the flame and  $D_f$  increases to 1.98 at 5 atm.

Keywords: soot, counterflow, pressurised flame, light scattering, morphology

 Supplementary material for this article is available [online](#)

(Some figures may appear in colour only in the online journal)

## 1. Introduction

Morphology of combustion generated soot particles has been extensively investigated in different flame configurations at atmospheric pressure, using intrusive and non-intrusive diagnostics [1–7]. Soot formation/oxidation processes in practical

combustion devices are influenced by the environment in which they occur. Therefore, it is important to investigate the morphological parameters of soot at conditions relevant to practical combustion systems. Gas turbines and diesel engines operate at high pressure and investigating soot morphology at elevated pressure is of practical relevance. In IC engines, an optical cylinder can provide a wide range of optical access and has been used to study soot at elevated pressures [8, 9]. However, in IC engines, combustion takes place in a highly turbulent environment with large variations in pressure and temperature throughout the cycle, making it difficult to isolate the pressure and fluid dynamics effects in such experiments.

<sup>1</sup> Author to whom any correspondence should be addressed.



Original content from this work may be used under the terms of the [Creative Commons Attribution 3.0 licence](#). Any further distribution of this work must maintain attribution to the author(s) and the title of the work, journal citation and DOI.

Soot measurements have also been carried out in shock tube experiments [10–12]. However, the residence time in shock tube experiments are much smaller compared to the diffusion based combustion devices [13]. Laminar non-premixed flames can be advantageous to study as the fluid dynamics is well characterized in these flames and influence of pressure can be isolated. Although, much control over the experimental conditions can be achieved in laminar flames but the necessity of wide angle optical access makes such experimental setups complex and increases safety risks related to pressure. The additional complexity of using laser diagnostics for soot studies makes this area of research unpleasant, leading to a knowledge gap of our understanding of the influence of pressure on pollutant formation. Most of the sooting flames studied at increased pressure are coflow flames and in those experiments optical access is restricted to one angle [14–16]. With the inherent restricted access in typical pressurized experimental apparatuses, intrusive techniques such as thermophoretic sampling (TS) followed by transmission electron microscopy (TEM) are necessary to provide information about morphological parameters of soot [17, 18]. However, such measurements can perturb the flame resulting in variation of the flow field, which can lead to experimental uncertainties [19]. Amin *et al* [17] used TS-TEM to investigate soot morphology in counterflow flames up to 10 atm. However, the soot field was not resolved along the axis of the burner due to small spatial extent of the soot zone, necessitating that the soot parameters be averaged over the entire soot zone.

Time resolved laser induced incandescence (TiRe-LII) is a non-intrusive diagnostic for investigating primary particle size distribution of soot and has been commonly used at atmospheric pressure [20–22]. However, at elevated pressures TiRe-LII has not been successfully applied for measuring the primary particle size distribution because of difficulties of accounting for the shielding effect in the analysis of heat conduction rate between aggregated particles and surrounding gas [14]. Multi-angle light scattering/extinction has also been used for *in situ* measurements of soot at atmospheric pressure [23–26] but has not been reported at high pressures. Koylu [27] presented a methodology for the measurement of soot concentration, primary particle size, aggregate size distribution and fractal dimension of soot from multi-angle light scattering and extinction measurements. To measure these parameters of soot, optical access from about 10 to 160° is required along with prior knowledge of fractal prefactor and refractive index of soot. According to authors' knowledge, neither a shock tube nor an experimental setup for pressurized flame studies with wide range of optical access for multi-angle light scattering has been reported.

In this work, a novel experimental setup is described which can provide the necessary optical access for multi-angle light scattering for investigating soot parameters. A pressure vessel has been designed and built in which four curved optical windows are installed. A counterflow burner is also designed and built which can produce steady, laminar and axis-symmetric flame in pressurized environment. Counterflow flames are 1D and allow for the control of residence time, which is very important for manipulating the soot loading in pressurized

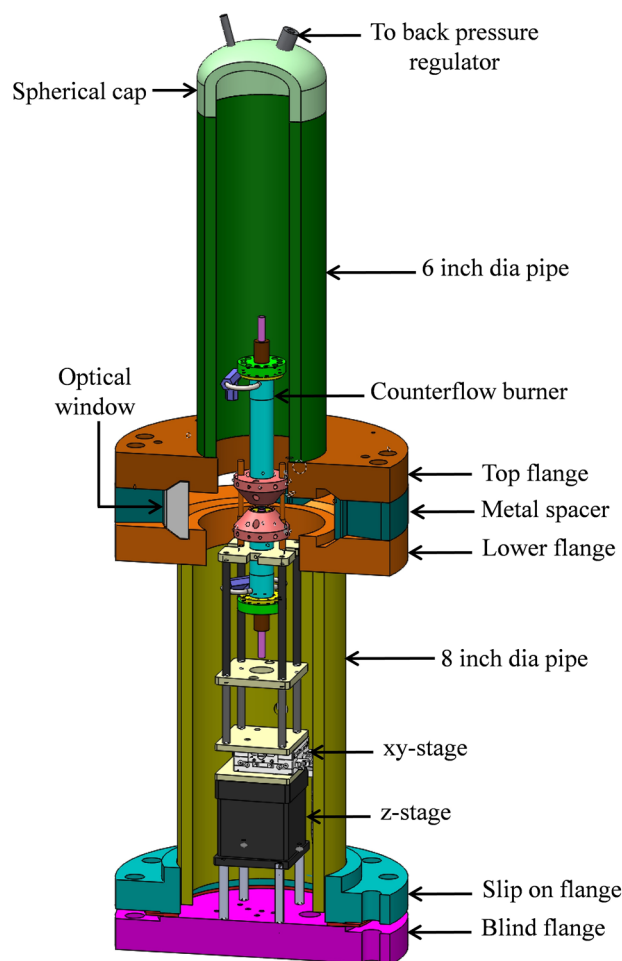


Figure 1. CAD drawing of burner and pressure vessel.

flames. Using this novel apparatus, moderately sooting flames of  $N_2$ -diluted ethylene and air are stabilized from 3 to 5 atm. An Ar/Kr ion laser is used to perform light scattering and extinction measurements. The light scattering signal is collected at regular intervals between 15° to 165° along different axial locations of the burner, at each pressure. Using Rayleigh–Debye–Gans theory for fractal aggregates (RDG-FA), values of soot volume fraction, primary particle size, mean aggregate size and fractal dimension of aggregate are calculated at elevated pressures.

## 2. Experimental apparatus

### 2.1. Pressure vessel

A state-of-the-art apparatus is designed and built specifically for studying soot morphology at high pressure. Figure 1 shows a CAD drawing of the pressure vessel and the counterflow burner placed inside the vessel. A brief description of this experimental apparatus is available in [28], however, a more detailed description is given here. The vessel has a height of 1.25 m to accommodate this counterflow burner as well as a laminar coflow burner. The section of the vessel is constructed of a 6-inch (150 mm) diameter, schedule 80 stainless steel pipe welded to a spherical cap on top while the other end of

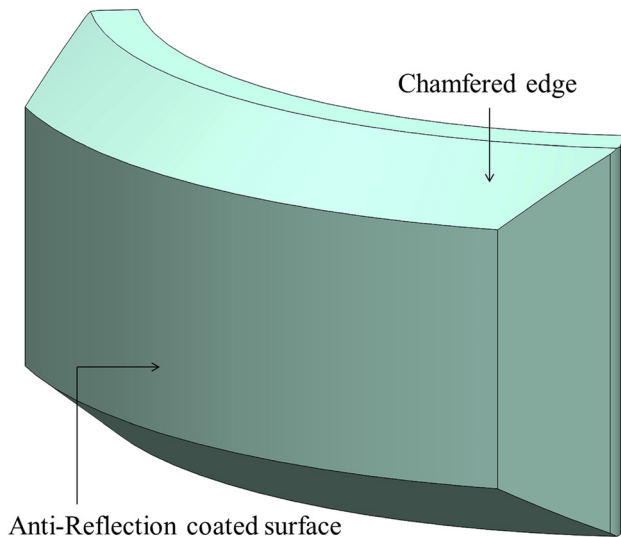


**Figure 2.** 3D sketch of the optical window.

the pipe is welded to a custom designed flange (top flange). The lower section of the vessel consists of an 8-inch diameter schedule 80 stainless steel pipe that is welded to another custom designed flange (lower flange). The pressure vessel has four curved windows, each providing an optical access of  $60^\circ$ . Optical windows were custom ground from optical grade fused silica and have an anti-reflection (AR) coating on both curved surfaces, (coating type: BBAR) for the wavelengths of 355–532 nm, as shown in figure 2. The edges are chamfered to promote sealing at pressure. These windows are placed in the grooves made in customized top and lower flanges of the vessel and both the flanges are separated by metal spacers in such a way that optical windows can float freely between them in a bed of silicon sealant. Once assembled, four curved windows provide  $0$  to  $180^\circ$  of optical access. The exhaust line of the pressure vessel is connected at the top of the pressure vessel. A blind flange closes the vessel at the lower end, where the burner is mounted. All the inlet flows are provided through the blind flange.

To facilitate the burner movement inside the pressure vessel for scanning the flame and fine alignment, the burner is mounted on 3-axis translation stages and these translation stages are mounted on the blind flange. A vertical translation stage (EKSMA Optics: 940-0210) has a stepper motor inside and can provide a travel range of 25 mm and resolution of  $0.625 \mu\text{m}$  in  $1/8$  step. A custom XY steel stage (Sigma-koki TSD-802SDL-SGDC) with remote actuators is mounted on the vertical translation stage. On the top of these XY-stages, base of the counterflow burner is attached. Electrical feed to these translation stages is provided through a KEMILON multi-pin connector (16-B-04097-12) which is inserted in the blind flange.

Figure 3 shows the schematic and actual photographs of the apparatus and the entire experimental setup. This figure has been used in [28], however, for clarity it has been modified here. Four complete sets of scattered light collection optics are attached to a rotary stage through four arms, allowing measurement at four angles simultaneously. This

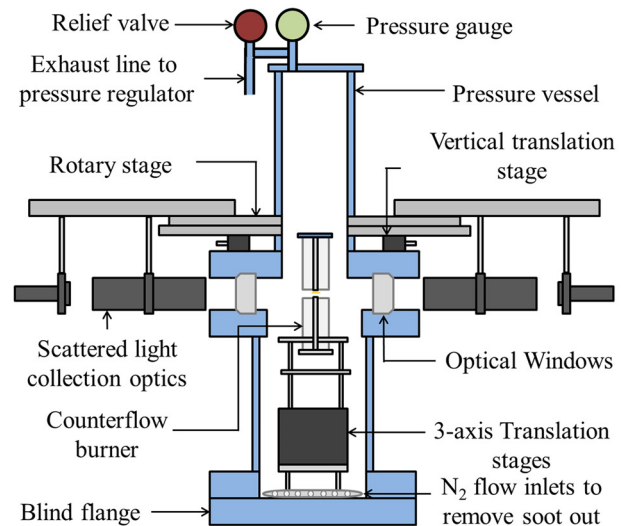


**Figure 3.** Schematic of pressure vessel with scattered light collection optics (top) and photograph of the experimental setup (bottom). Reprinted from [28]. Copyright 2017, with permission from Elsevier.

rotary stage is supported on four miniature vertical translation stages attached to the pressure vessel to allow fine alignment of the rotary stage in the horizontal plane. The rotary stage enables collecting the scattered light at different angles. To prevent soot accumulation on the windows at high soot loadings without perturbing the flame, an evenly distributed curtain of nitrogen flows around the windows inside the vessel from a circular ring attached to the blind flange at the bottom of the vessel.

The exhaust line from the top of the pressure vessel is connected to a dome loaded backpressure regulator (BPR) (Equilibar: GSD4—SS316 NR HP1500), which is controlled by an electronic pressure regulator (GPI series—single loop). The desired pressure inside the pressure vessel is set through a LABVIEW program which regulates the electronic pressure regulator, and hence the pressure on the dome side of the BPR.

The pressure inside the vessel is also monitored by a digital pressure gauge. A spring loaded pressure relief valve is also connected at the top of the pressure vessel in the event of an over pressurization.

## 2.2. Counterflow burner

The counterflow burner detailed here has been used in [17], which consists of two concentric straight tubes having an internal diameter of 8.5 mm. The diameter ( $D$ ) of the burner is less than the ones that have been commonly used for experiments at atmospheric pressures. This diameter is chosen in order to reduce the inlet flows and hence the soot loadings. For the counterflow flame to be adiabatic, the separation distance ( $H$ ) between two nozzles should correspond to  $1 < H/D < 2$  [29]. Considering this requirement, opposed tubes of the burner are separated by 8.0 mm, which is kept constant. Figure 4 shows the 2D sketch of one half of the burner. Outer tubes surround main flow tubes to provide a coflow of nitrogen. At the supply end of these tubes, custom-made hollow flanges are welded and the ends are closed with blind flanges. The blind flange and a hollow flange have a groove in which an O-ring is placed. This O-ring not only provides sealing but also allows centering the main flow tube with the outer tube by adjusting the torque on the screws used to couple hollow and blind flange.

Flow conditioners have been used to provide a top-hat velocity profile and produce a flat flame. RECEMAT™ foam is added in the main flow tubes and five mesh screens are added on top of this, each separated by a retaining ring of 1 mm height as shown in figure 4. These retaining rings have been made using wire EDM and have a thickness of 0.25 mm, allowing the meshes to sit without warping. As the Reynolds number increase, the edges of the flames become asymmetric due to the shear layer between the inner flow and the coflow. To overcome this, meshes are also added to the top of RECEMAT foam in the coflow tubes to try and mitigate this shear layer.

## 3. Experimental procedure

Ethylene and nitrogen having a mole fraction of 0.35 and 0.65, respectively, are introduced from the bottom tube while the air is supplied from the top tube of the burner. A global strain rate, which is the ratio of half of the mean velocity of air at the exit of the nozzle to separation distance between nozzles, is maintained at  $30\text{ s}^{-1}$  at all pressures by adjusting the inlet fluxes [30]. A velocity-matched coflow of nitrogen is provided to prevent the entrainment from surroundings. The flame studied is a soot formation (SF) flame and is located on the oxidizer side of the stagnation plane. Visual observation of the flames showed that the flames are axisymmetric and flat; essential for performing multi-angle light scattering measurements in counterflow flames.

Ar/Kr Ion laser can emit several wavelengths in the visible range simultaneously, which is why it has been chosen with this setup. Using the multi-wavelength mode of the laser, the refractive index of soot will be investigated in pressurized

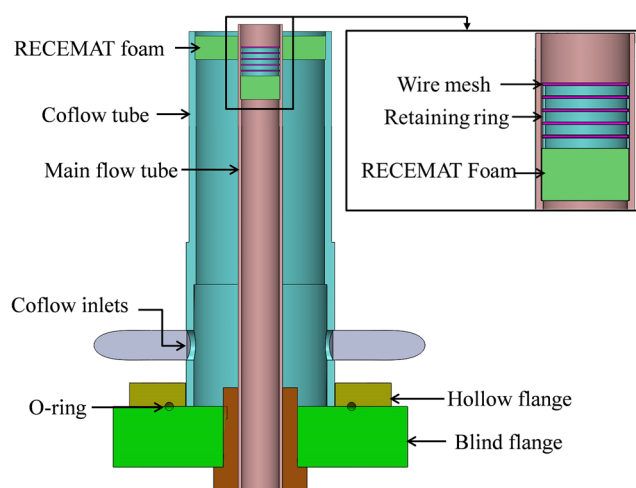


**Figure 4.** Sectional view of the modified nozzle of counterflow burner and detailed view showing wire mesh held on retaining ring.

flames. For multi-angle light scattering measurements, a vertically polarized beam at a wavelength of 514.5 nm has been used. The beam is focused to a beam waist diameter of  $100\ \mu\text{m}$ , at the center of the flame, using a combination of optics. The attenuated laser beam is focused into an integrating sphere on which a laser line filter and a photo detector are mounted. A reference laser signal is measured to take into account any fluctuations in laser power. This reference signal does not pass through the pressure vessel as passing the laser beam through the vessel hinders the optical access for scattering measurements at some angles. Moreover, soot accumulation in the vessel or on the optical windows was negligible and did not influence the laser extinction signal. The light scattering measurement setup used here is same as the one used in [28], except the pinhole is replaced with a slit and four detectors were used simultaneously to measure the light scattering from soot particles.

To perform multi-angle light scattering, the center of rotation of the collection optics mounted on rotary stage must be aligned with the center of the burner. The scattered light is measured between  $15^\circ$  to  $165^\circ$  using four detectors at an increment of  $5^\circ$  and alignment of the center of burner with center of the rotary stage is vital as it allows to correctly quantify the signal trapping of scattered signal from soot particles. A misalignment will result in mismatch of scattering trends measured by each light collection optics. These collection optics are mounted outside the pressure vessel while the burner is inside the vessel and this fine alignment can be a challenging and time-consuming task. A custom designed pin is placed on the lower part of the counterflow burner as shown in figure 5(a). The laser beam is splitted into two and one of the beams is then termed the incident beam and the other one is termed second beam as shown in figure 5(b). The precise center of the rotary stage is located by passing the two laser beams at right angle, along the diameter of rotary stage. Incident and second laser beams are in the same horizontal plane. The pin tip is moved to the intersection point using the  $xy$ -translation stages and the second laser beam is simply blocked without removing the beam splitter. Incident laser beam hits the tip of

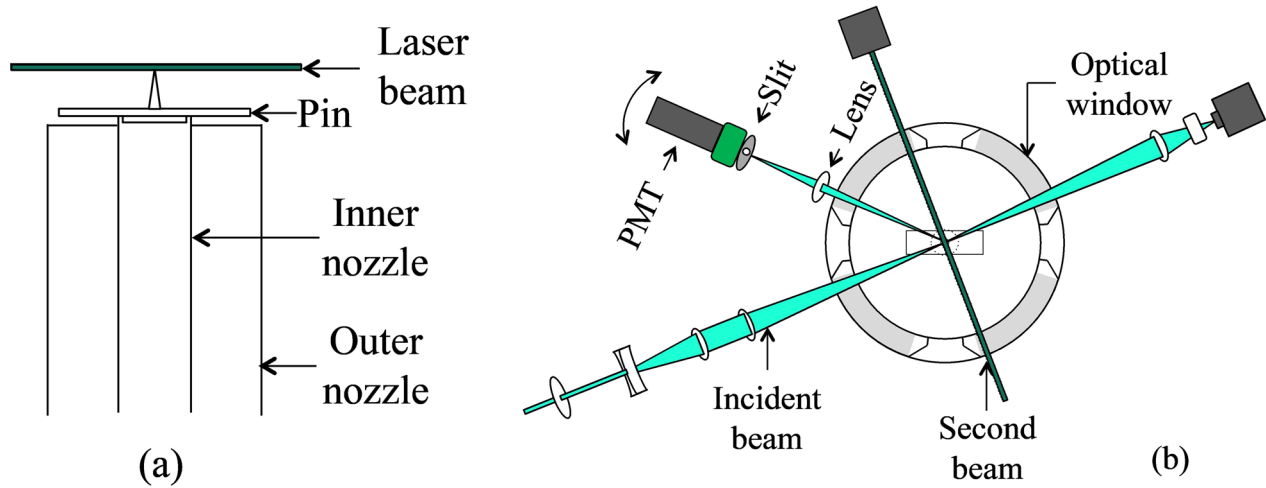


Figure 5. Scattering pin positioned on burner (a), laser beams intersecting the pins (b).

the pin and scattered light by the pin is focused on the slit of scattering light collection optics and alignment adjustments are made until the scattered light remains in focus on the slit while the rotary stage is rotated.

Scattered light by the soot particles is collected by a set of four light collection optics, which can be placed at desired angles by rotating the rotary stage. A schematic of laser diagnostic is shown in figure 6. A biconvex lens which acts as a scattered light collection lens, collects the scattered light and focuses it to a slit of 50 μm width. The slit has a height of 3 mm and is used to mitigate the effects of change in alignment of optics in vertical direction due to rotation of the rotary stage. Depolarized light is filtered out by a polarizer mounted in front of the slit. To minimize the effect of surrounding light and flame radiation, a laser line filter is used in front of the photo multiplier tube (PMT) and the signal is measured by using a lock-in-amplifier.

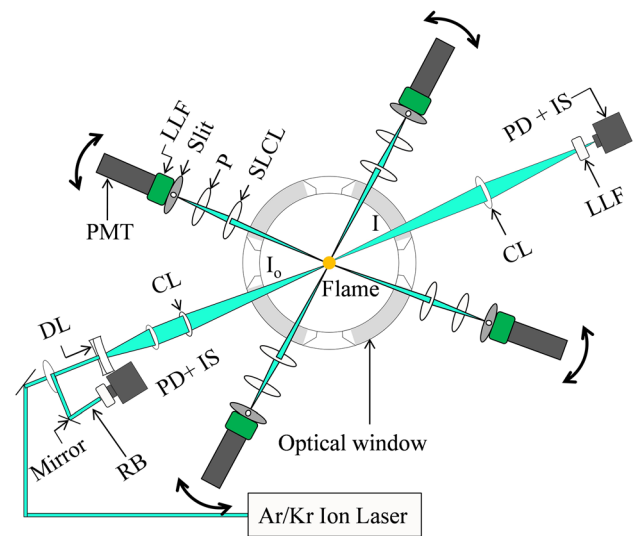


Figure 6. Schematic of laser diagnostic, CL = converging lens, DL = diverging lens, IS = integrating sphere, LLF = laser line filter, P = polarizer, PD = photodiode, PMT = photo multiplier tube, RB = reference beam, SLCL = Scattered light collection lens. Reprinted from [28]. Copyright 2017 with permission from Elsevier.

## 4. Theory

### 4.1. Multi-angle light scattering

Details of RDG-FA theory for calculating soot parameters from multi-angle light scattering measurements are given in [24, 27, 31]. Only brief procedure is described here. From the measured scattering intensities of soot ( $I_{vv}(\theta)$ ), the scattering coefficients of soot  $K_{vv}(\theta)$  at each angle are calculated using

$$K_{vv}(\theta) = K_{vv}^{\text{gas}} \frac{I_{vv}(\theta)}{I_{vv}^{\text{gas}}}. \quad (1)$$

$K_{vv}^{\text{gas}}$  is the known scattering coefficient of calibration gas and  $I_{vv}^{\text{gas}}$  is the measured scattering intensity of calibration gas at each angle. Propane is used as a calibration gas and to account for the background signal and internal reflections from the wall, scattering from nitrogen is also measured. The scattering signal is measured at several angles between 15° to 165° while scattering in forward and backward directions are not possible to measure due to physical constraints of the experimental setup.  $K_{vv}(\theta)$  values in forward and backward directions are calculated by extrapolating the known

scattering behaviour of soot. Total scattering contribution  $K_{\text{sca}}$  is calculated by integrating scattered light over 4π solid angle by the following relation

$$K_{\text{sca}} = \int_{\theta=0}^{2\pi} \int_{\theta=0}^{\pi} K_{vv}(\theta) \left( \frac{1 + \cos^2(\theta)}{2} \right) \sin \theta d\theta d\phi. \quad (2)$$

Absorption coefficients ( $K_{\text{abs}}$ ) are calculated by subtracting the total scattering coefficient from the measured extinction coefficients ( $K_{\text{ext}}$ ). Where  $K_{\text{ext}}$  can be calculated from Beer's Law

$$K_{\text{ext}} = -\frac{1}{L} \ln \frac{I}{I_0}. \quad (3)$$

$I_0$  and  $I$  are the incident and transmitted light intensities and  $L$  is the length of soot zone which is measured by imaging the soot luminosity. From  $K_{\text{ext}}$ , path averaged soot volume fraction is measured using the following

$$f_v = \frac{\lambda}{6\pi E} \frac{K_{\text{ext}}}{1 + \rho_{\text{sa}}} \quad (4)$$

$\lambda$  is the wavelength of the incident light.  $E = \text{Im}[(m^2 - 1) / (m^2 + 2)]$  where  $m$  is the refractive index of soot. Krishnan *et al* [32] reported  $m = 1.62 + 0.66i$  for the wavelength used in this study and  $E = 0.29\% \pm 0.27\%$  corresponding to the chosen refractive index has been used for the current work at all pressures. According to mass fractal relationship soot aggregates are described by the equation

$$N = k_f \left( \frac{2R_g}{d_p} \right)^{D_f} \quad (5)$$

$N$  is the number of primary particles in an aggregate and  $k_f$  is the fractal prefactor. RDG-FA relate the optical cross sections to particle/aggregate size and morphology. According to RDG-FA theory, optical scattering cross section of an aggregate is

$$C_{\text{vv}} = N^2 C_{\text{vv}}^p f(qR_g) \quad (6)$$

Where  $q = 4\pi \sin(\theta/2) / \lambda$  and  $C_{\text{vv}}^p$  is the scattering cross section of the individual primary particle in Rayleigh limit ( $d_p \ll \lambda$ ).  $f(qR_g)$  is the optical form factor of an aggregate. Average form factor for fractal aggregates is

$$f(qR_g) = \begin{cases} \exp\left(-\frac{q^2 R_g^2}{3}\right) & \text{Guinier Regime} \\ (q^2 R_g^2)^{-D_f/2} & \text{Power-Law regime} \end{cases} \quad (7)$$

For the analysis of soot aggregates, Guinier and Power-Law regimes are considered for  $qR_g \leq 1$  and  $qR_g > 1$ , respectively [33]. In Guinier regime, variation of scattering in angular direction is

$$\frac{I_{\text{vv}}(\theta)}{I_{\text{vv}}(0^\circ)} = 1 - \frac{q^2 \overline{R_g^2}}{3} \quad (8)$$

$\overline{R_g^2}$  is the mean squared radius of gyration and can be determined from the linear slope of  $K_{\text{vv}}(0^\circ)/K_{\text{vv}}(\theta_G)$  versus  $q^2$  where the linear slope of the plot yields  $\overline{R_g^2}/3$ . According to RDG-FA theory, scattering coefficient in the power law regime varies according to

$$K_{\text{vv}}(\theta) = n_p C_{\text{vv}}^p \frac{k_f}{(qd_p/2)^{D_f}} \quad (9)$$

$n_p$  is the number density of primary particles. The striking feature of equation (9) is that it does not depend on aggregate size but varies only due to  $q$  and slope of log-log plot of  $K_{\text{vv}}(\theta)/K_{\text{abs}}$  versus  $q$  leads to the determination of fractal dimension. Using the scattering coefficient at  $145^\circ$  in the power-law regime, mean particle size is calculated using the relation

$$d_p = \frac{\lambda}{\pi} \left[ 4\pi \frac{E}{F} \frac{K_{\text{vv}}(\theta_L)}{K_{\text{abs}}} \frac{(2 \sin \theta_L/2)^{D_f}}{k_f} \right]^{1/(3-D_f)} \quad (10)$$

$k_f$  equal to 2.0 has been used for this work as this value has been reported under various conditions of combustion [1] and

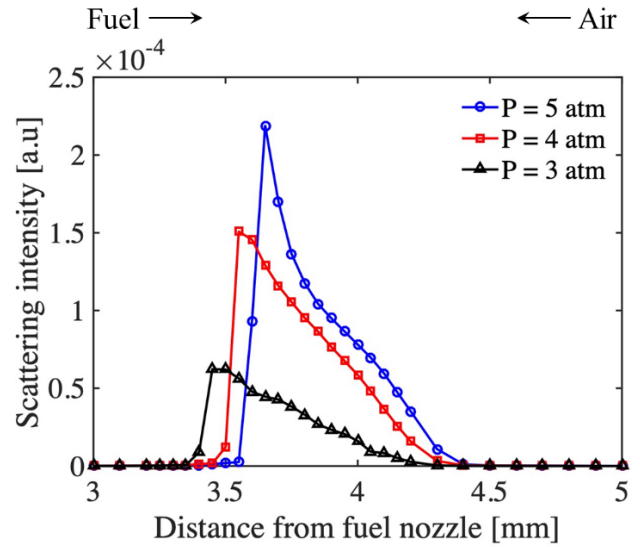


Figure 7. Scattering intensities of soot particles measured at an angle of  $90^\circ$  at different pressures.

$F = |(m^2 - 1) / (m^2 + 2)|^2$ . For the chosen refractive index,  $F$  is  $0.27\% \pm 44\%$  [32].

## 5. Results

### 5.1. Soot scattering intensities at $90^\circ$

Figure 7 shows the scattering intensities by soot particles measured along the axis of the flame from 3 to 5 atm. At 1 and 2 atm, it is not possible to accurately perform multi-angle light scattering due to low soot loading at these highly diluted conditions. The particle stagnation plane is located on the left of the peak scattering intensities. The flames are located near the start of increase in scattering intensities on the right side of the graphs. Scattering signal is measured at  $90^\circ$  and is seen to increase as the particles move from the near flame region towards the stagnation plane. Scattering intensities reach a maximum value and then decrease sharply as the particles are convected away radially at stagnation plane. Due to the slight curvature effects of the flame, the location of the peak scattering intensity seems to shift away from fuel nozzle as the pressure is increased from 3 to 5 atm. In the following discussion, multi-angle light scattering measurements will be presented as a function of the distance from peak scattering intensity at each pressure.

### 5.2. Multi-angle light scattering measurements

Figure 8 shows the ratio of scattering to absorption coefficients at different axial locations measured at pressures from 3 to 5 atm. Plots on the left side (a)–(c) of figure 8 show ratio of scattering to absorption coefficients versus the scattering angle in log-linear space at various locations from the peak scattering signal at each pressure. This ratio is seen to increase as the particles move towards the peak scattering location

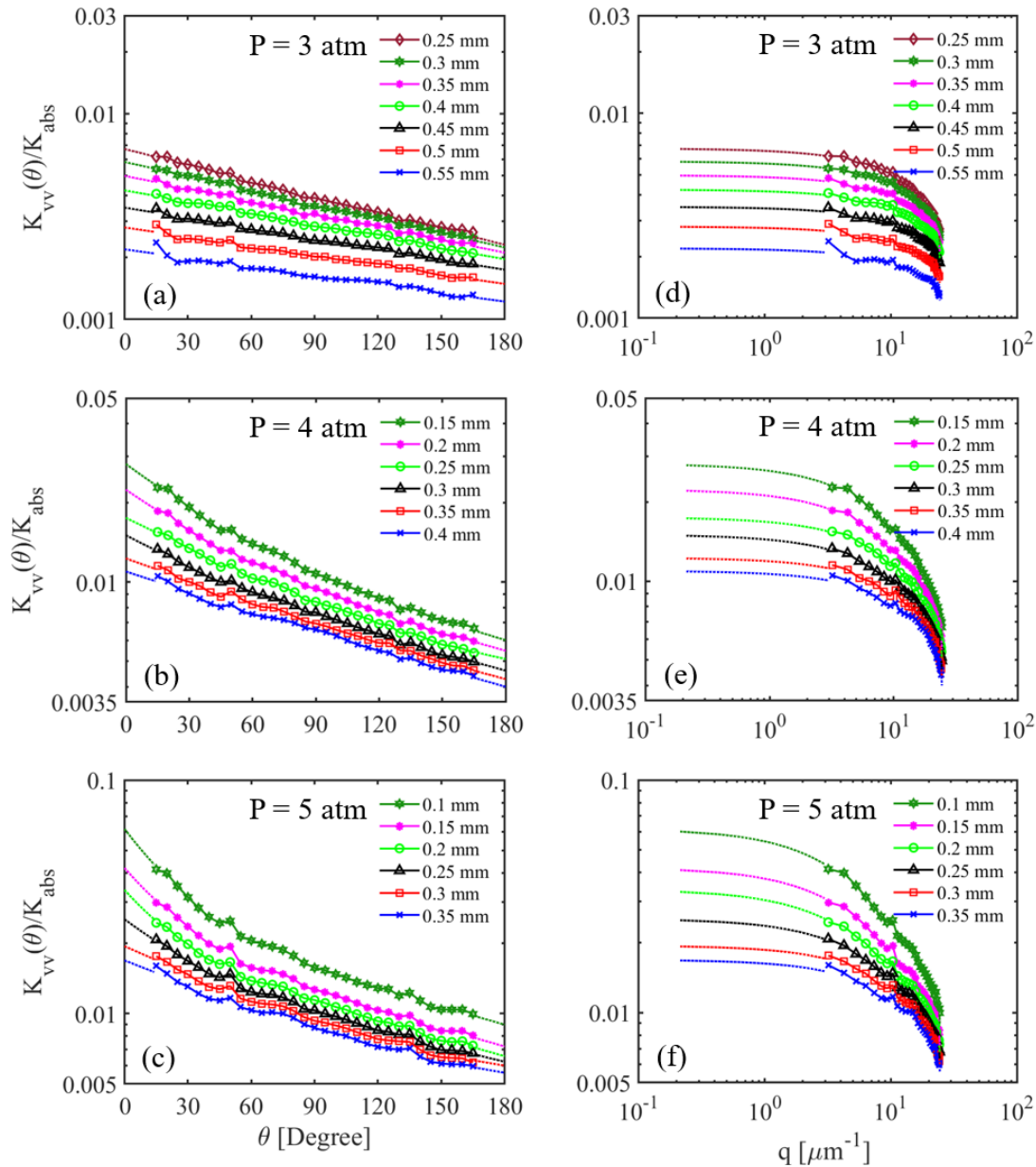


**Figure 8.** Ratio of scattering to absorption coefficients versus the scattering angle (left (a–c)) and the ratio of scattering to absorption coefficients versus  $q$  (right (d–f)) at different pressures along the flame axis. Dotted lines show the extrapolation of scattering at small and large angles whereas the legend shows distance from peak scattering signal on the air side.

at each pressure due to changes in soot morphology. The increase in  $K_{VV}(\theta)/K_{abs}$  at large angles is due to an increase in primary particle diameter. Plots on the right side (d–f) of figure 8, shows the log–log plots of the  $K_{VV}(\theta)/K_{abs}$  versus the modulus of the scattering vector ( $q$ ) at various locations from the peak scattering signal at each pressure. The slope of the line at angles corresponding to power-law regime gives the fractal dimension of the soot aggregates. Variation of scattering contribution relative to absorption at different pressures is presented here. Small irregularities exist at  $50^\circ$  and  $130^\circ$  due to slightly restricted optical access at those angles.

The increase in area under each plot represents an increase in scattering contribution compared to absorption. The ratio  $K_{sca}/K_{abs}$  is called scattering to absorption ratio ( $\rho_{sa}$ ) whereas the ratio of scattering to extinction coefficients is called albedo

( $\omega_A = \rho_{sa}/(1 + \rho_{sa})$ ) and both can be estimated through multi-angle light scattering measurements.

The values of  $\rho_{sa}$  and  $\omega_A$  are obtained at several heights along the axis of the burner from 3 to 5 atm as shown in figure 9. Both  $\rho_{sa}$  and  $\omega_A$  increase at each pressure along the burner axis as the soot particles move towards the peak scattering signal location from the near flame region. Moreover,  $\rho_{sa}$  and  $\omega_A$  increase with pressure and maximum value of  $\rho_{sa}$  at 3 atm increases from 0.03 to 0.16 at 5 atm for the measurements presented here. These variations can be due to change in primary particle diameter and/or aggregate morphology.  $\rho_{sa}$  is particularly sensitive to a change in primary particle diameter [15] and depending on the morphology of soot, it can be as large as 0.9 for the wavelength in the visible range [34]. Soot particle size changes significantly with pressure [17, 18,



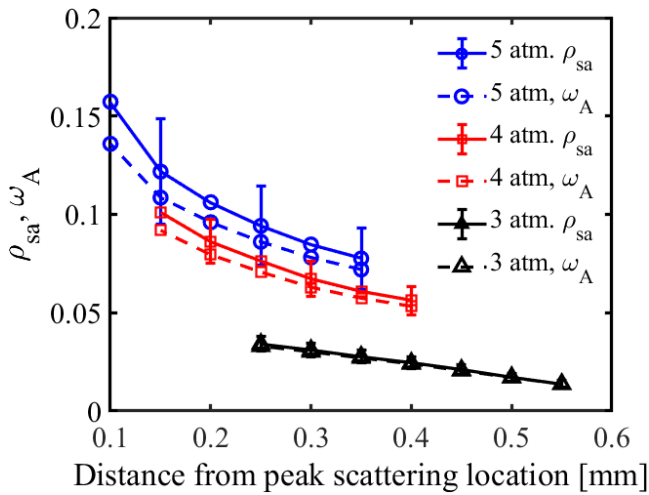


Figure 9. Scattering to absorption ratio ( $\rho_{sa}$ ) and albedo ( $\omega_A$ ) at different pressures along the burner axis.

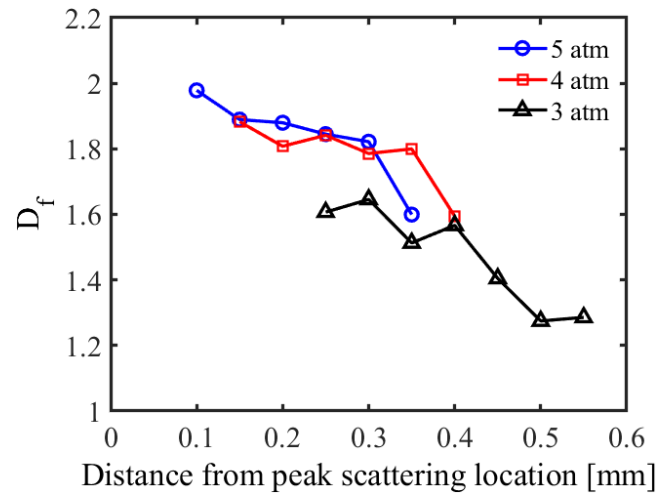


Figure 11. Fractal dimension of soot aggregates at different pressures along the burner axis.

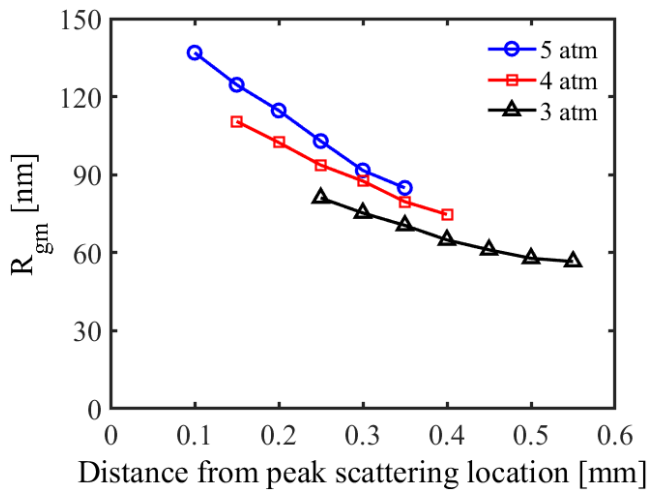


Figure 10. Radius of gyration of soot aggregates at different pressures along the burner axis.

35]. Therefore,  $\rho_{sa}$  is important parameter when light scattering and extinction are used for the measurement of soot concentration and particle size.

We obtain the measured radius of gyration of soot aggregates ( $R_{gm} = \overline{R_g^2}$ ) by making a linear fit to the plots of  $K_{vv}(10^\circ)/K_{vv}(\theta_G)$  versus  $q^2$  and these plots are shown in supplementary material (figure 1S) ([stacks.iop.org/MST/30/075902/mmedia](https://stacks.iop.org/MST/30/075902/mmedia)).  $10^\circ$  has been used as a smallest angle because the value of  $K_{vv}(0^\circ)$  is not measured but it is extrapolated and choosing  $0^\circ$  as the smallest angle can add uncertainties. Furthermore, choice of  $10^\circ$  as smallest angles has often been used [24]. Figure 10 shows the quantitative values of measured radius of gyration with an uncertainty of 6%. Radius of gyration increases as the soot particles move from the near flame region towards the peak scattering signal and  $R_{gm}$  also increases considerably with pressure.

Fractal dimension ( $D_f$ ) of soot aggregates are obtained by making the linear fits to the log–log plot of  $K_{vv}(\theta)/K_{abs}$  versus  $q$  (figures 8(d)–(f)) for angles between  $120^\circ$  to  $165^\circ$  which correspond to the values of  $q$  from  $21.2$  to  $24.2 \mu\text{m}^{-1}$  for the

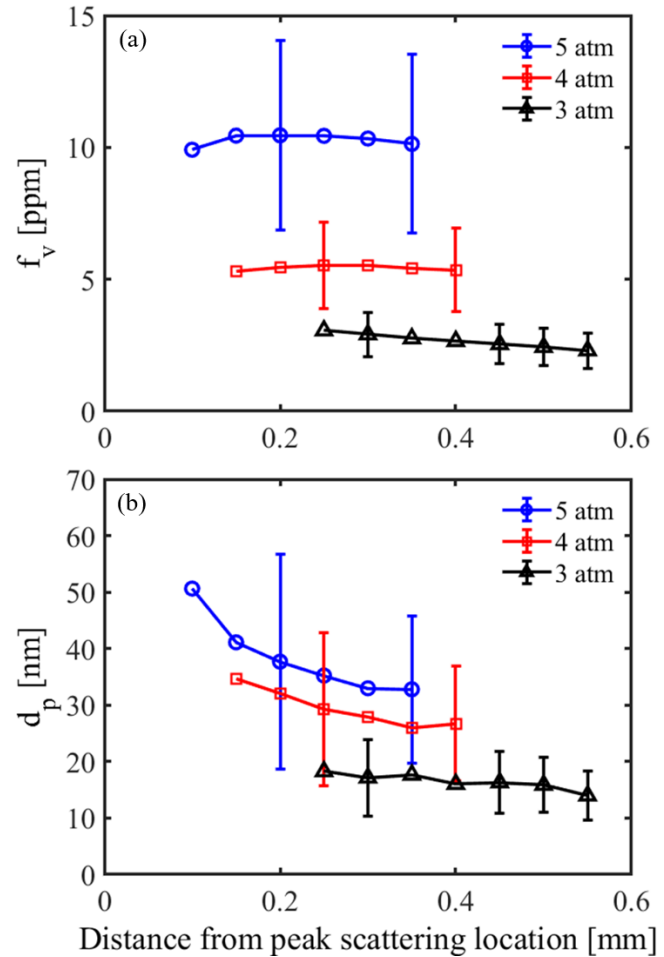


Figure 12. Path averaged soot volume fraction ( $f_v$ ) (a) and mean primary particle size ( $d_p$ ) (b) at different pressures along the burner axis.

wavelength of  $514.5 \text{ nm}$ . Figure 11 shows the  $D_f$  values along the flame axis at each pressure and the reported values have an uncertainty of 8%.  $D_f$  is small near the flame and its value increases at each pressure as the particles move from the near flame region towards the peak scattering signal. Values of  $D_f$

in figure 11 vary from 1.27 to 1.6 at 3 atm whereas fractal dimension does not change significantly as the pressure is increased from 4 to 5 atm and maximum value of  $D_f$  at 5 atm is 1.98. For the determination of  $D_f$ , fitting interval has been chosen where  $qR_g > 1$  [33]. Oltmann *et al* [26] has discussed the criteria for fitting interval where  $qR_g$  values range between 1.6 and 5. At 3 atm, aggregates near the flame satisfy the condition of  $qR_g > 1$  but they may not fulfill the criteria of  $qR_g > 1.6$ . In a recent study by Gigone *et al* [18] fractal dimension is reported to increase as a function of the height above the burner (HAB) in coflow flames. Their reported  $D_f$  values vary from 1.2 to 1.96 at various HAB and at different pressures. In another study by Amin *et al* [17],  $D_f$  is averaged over the entire soot zone in counterflow flames and its values ranged between 1.61 to 1.67 without following any specific trend with pressure.

Figures 12(a) and (b) shows the path averaged soot volume fraction ( $f_v$ ) and mean primary particle size ( $d_p$ ) at various pressures along the flame axis.  $f_v$  increases significantly as the pressure is increased from 3 to 5 atm whereas its value also changes at each pressure as the particles move from the near flame region towards the peak scattering location. Error bars show the uncertainties due to absorption path length, detector's response and refraction index function,  $E(m)$ .  $d_p$  shows similar trends with pressure and increases as the pressure is raised.  $d_p$  also increases at each pressure as the particles are convected away from the near flame region. These results are consistent with our previous study [28]. Major sources of uncertainties for particle size measurement are  $E(m)$ ,  $F(m)$ , and scattering and absorption coefficients.

## 6. Conclusions

To investigate the morphological parameters of soot using multi-angle light scattering and extinction measurements, a state-of-the-art experimental setup was designed and built. The experimental setup consists of a counterflow diffusion flame burner inside a pressure vessel which can provide optical access from nearly  $0^\circ$  to nearly  $180^\circ$  for the measurement of laser light scattering by soot particles. As an example, a  $N_2$ -diluted ethylene and air laminar axisymmetric counterflow flame at elevated pressures was probed. Multi-angle light scattering measurements are performed and the light scattering signal by soot particles is collected between  $15^\circ$  to  $165^\circ$  at an interval of  $5^\circ$ .

Total scattering to absorption ratio increases with pressure and the maximum value of 0.03 at 3 atm increases to 0.16 at 5 atm. For accurately estimating the soot concentration and primary particle size using a simple light scattering and extinction technique, the contribution of scattering relative to absorption needs to be estimated.

Path averaged soot volume fraction ( $f_v$ ), mean primary particle size ( $d_p$ ) and radius of gyration ( $R_{gm}$ ) of soot aggregates increase with pressure and these trends are consistent with the results reported by Amin *et al* [28].

Fractal dimension of soot particles has a low value of 1.27 near the flame region, however at each pressure,  $D_f$  value increases as the soot particles move towards peak scattering signal and maximum value of 1.98 is inferred at 5 atm which is close to universally accepted value of 1.9 [18].

Multi-angle measurements such as these are helpful in understanding the influence of pressure on soot morphology and this setup can be used to study soot morphology in counterflow and coflow flames at elevated pressures.

## Acknowledgment

The authors acknowledge the financial support from King Abdullah University of Science and Technology (KAUST).

## ORCID iDs

Hafiz M F Amin  <https://orcid.org/0000-0002-6382-757X>

## References

- [1] Hu B, Yang B and Koylu U O 2003 Soot measurements at the axis of an ethylene/air non-premixed turbulent jet flame *Combust. Flame* **134** 93–106
- [2] Kempema N J and Long M B 2016 Combined optical and TEM investigations for a detailed characterization of soot aggregate properties in a laminar coflow diffusion flame *Combust. Flame* **164** 373–85
- [3] Koylu U O, Xing Y and Rosner D E 1995 Fractal morphology analysis of combustion-generated aggregates using angular light scattering and electron microscope images *Langmuir* **11** 4848–54
- [4] Köylü Ü Ö and Faeth G M 1992 Structure of overfire soot in buoyant turbulent diffusion flames at long residence times *Combust. Flame* **89** 140–56
- [5] Sorensen C M, Cai J and Lu N 1992 Light-scattering measurements of monomer size, monomers per aggregate, and fractal dimension for soot aggregates in flames *Appl. Opt.* **31** 6547–57
- [6] Wang Y-F, Huang Q-X, Wang F, Chi Y and Yan J-H 2017 Effects of morphology and wavelength on the measurement accuracy of soot volume fraction by laser extinction *Meas. Sci. Technol.* **29** 015202
- [7] Krüger V, Wahl C, Hadeff R, Geigle K P, Stricker W and Aigner M 2005 Comparison of laser-induced incandescence method with scanning mobility particle sizer technique: the influence of probe sampling and laser heating on soot particle size distribution *Meas. Sci. Technol.* **16** 1477
- [8] Stevens E and Steeper R 2001 Piston wetting in an optical DISI engine: fuel films pool fires, and soot generation *SAE Technical Paper* 2001-01-1203 (<https://doi.org/10.4271/2001-01-1203>)
- [9] Koegl M, Hofbeck B, Will S and Zigan L 2018 Investigation of soot formation and oxidation of ethanol and butanol fuel blends in a DISI engine at different exhaust gas recirculation rates *Appl. Energy* **209** 426–34
- [10] Bonczyk P 1979 Measurement of particulate size by *in situ* laser-optical methods: a critical evaluation applied to fuel-pyrolyzed carbon *Combust. Flame* **35** 191–206

- [11] Di Stasio S, Massoli P and Lazzaro M 1996 Retrieval of soot aggregate morphology from light scattering/extinction measurements in a high-pressure high-temperature environment *J. Aerosol Sci.* **27** 897–913
- [12] Utsav K, Beshir M and Farooq A 2017 Simultaneous measurements of acetylene and soot during the pyrolysis of ethylene and benzene in a shock tube *Proc. Combust. Inst.* **36** 833–40
- [13] Karatas A E and Gülder Ö L 2012 Soot formation in high pressure laminar diffusion flames *Prog. Energy Combust. Sci.* **38** 818–45
- [14] Thomson K A, Snelling D R, Smallwood G J and Liu F 2006 Laser induced incandescence measurements of soot volume fraction and effective particle size in a laminar co-annular non-premixed methane/air flame at pressures between 0.5–4.0 MPa *Appl. Phys. B* **83** 469–75
- [15] Bennett A, Amin H M F, Cenker E and Roberts W L 2018 Measurements of pressure effects on PAH distribution and 2D soot volume fraction diagnostics in a laminar non-premixed coflow flame *Energy Fuels* **32** 10974–83
- [16] Steinmetz S A, Fang T and Roberts W L 2016 Soot particle size measurements in ethylene diffusion flames at elevated pressures *Combust. Flame* **169** 85–93
- [17] Amin H M F, Bennett A and Roberts W L 2019 Determining fractal properties of soot aggregates and primary particle size distribution in counterflow flames up to 10 atm *Proc. Combust. Inst.* **37** 1161–8
- [18] Gigone B, Karatas A E and Gülder Ö L 2019 Soot aggregate morphology in coflow laminar ethylene diffusion flames at elevated pressures *Proc. Combust. Inst.* **37** 841–8
- [19] Lee J, Altman I and Choi M 2008 Design of thermophoretic probe for precise particle sampling *J. Aerosol Sci.* **39** 418–31
- [20] Boiarciuc A, Foucher F and Mounaïm-Rousselle C 2006 Soot volume fractions and primary particle size estimate by means of the simultaneous two-color-time-resolved and 2D laser-induced incandescence *Appl. Phys. B* **83** 413–21
- [21] Tian B, Zhang C, Gao Y and Hochgreb S 2017 Planar 2-color time-resolved laser-induced incandescence measurements of soot in a diffusion flame *Aerosol. Sci. Technol.* **51** 1345–53
- [22] Sun Z, Gu D, Nathan G, Alwahabi Z and Dally B 2015 Single-shot, time-resolved planar laser-induced incandescence (TiRe-LII) for soot primary particle sizing in flames *Proc. Combust. Inst.* **35** 3673–80
- [23] Faeth G M and Koçylu U O 1994 Optical properties of overfire soot in buoyant turbulent diffusion flames at long residence times *J. Heat Transfer* **116** 152–9
- [24] Ma B and Long M B 2014 Combined soot optical characterization using 2D multi-angle light scattering and spectrally resolved line-of-sight attenuation and its implication on soot color-ratio pyrometry *Appl. Phys. B* **117** 287–303
- [25] Link O, Snelling D, Thomson K and Smallwood G 2011 Development of absolute intensity multi-angle light scattering for the determination of polydisperse soot aggregate properties *Proc. Combust. Inst.* **33** 847–54
- [26] Oltmann H, Reimann J and Will S 2012 Single-shot measurement of soot aggregate sizes by wide-angle light scattering (WALS) *Appl. Phys. B* **106** 171–83
- [27] Koçylu U O 1997 Quantitative analysis of *in situ* optical diagnostics for inferring particle/aggregate parameters in flames: implications for soot surface growth and total emissivity *Combust. Flame* **109** 488–500
- [28] Amin H M F and Roberts W L 2017 Soot measurements by two angle scattering and extinction in an N<sub>2</sub>-diluted ethylene/air counterflow diffusion flame from 2 to 5 atm *Proc. Combust. Inst.* **36** 861–9
- [29] Figura L and Gomez A 2012 Laminar counterflow steady diffusion flames under high pressure ( $P \leq 3$  MPa) conditions *Combust. Flame* **159** 142–50
- [30] Sung C J, Li B, Wang H and Law C K 1998 Structure and sooting limits in counterflow methane/air and propane/air diffusion flames from 1 to 5 atmospheres *Proc. Combust. Inst.* **27** 1523–9
- [31] Xing Y, Koçylu U O and Rosner D E 1999 *In situ* light-scattering measurements of morphologically evolving flame-synthesized oxide nanoaggregates *Appl. Opt.* **38** 2686–97
- [32] Krishnan S S, Lin K-C and Faeth G M 2000 Optical properties in the visible of overfire soot in large buoyant turbulent diffusion flames *J. Heat Transfer* **122** 517–24
- [33] De Iuliis S, Maffi S, Cignoli F and Zizak G 2011 Three-angle scattering/extinction versus TEM measurements on soot in premixed ethylene/air flame *Appl. Phys. B* **102** 891–903
- [34] Krishnan S, Lin K-C and Faeth G M 2001 Extinction and scattering properties of soot emitted from buoyant turbulent diffusion flames *J. Heat Transfer* **123** 331–9
- [35] Vargas A M and Gülder Ö L 2016 Pressure dependence of primary soot particle size determined using thermophoretic sampling in laminar methane-air diffusion flames *Proc. Combust. Inst.* **36** 975–84